Tribology International 219 (2026) 111778

Contents lists available at ScienceDirect

Tribology International

journal homepage: www.elsevier.com/locate/triboint

Full Length Article

Finite element modal analysis of a twin-disc tribometer: Sensitivity analysis and experimental validation using vibrometry

G. Brunbauer [a,d], M.J. Hochrainer [b], S. Krenn [a], A.M. Puhwein [a], M.S. Bonney [c], S.J. Eder [a,d,*], P.A. Fotiu [b]

[a] AC2T research GmbH, Viktor Kaplan-Straße 2/c, Wiener Neustadt, 2700, Austria
[b] Fachhochschule Wiener Neustadt GmbH, Johannes Gutenberg-Straße 3, Wiener Neustadt, 2700, Austria
[c] Faculty of Science and Engineering, Swansea University, Swansea Bay Campus, Swansea, SA1 8EN, United Kingdom
[d] Institute for Engineering Design and Product Development, TU Wien, Lehárgasse 6 – Objekt 7, Wien, 1060, Austria

ARTICLE INFO

Keywords:
Twin-disc tribometer
Finite element analysis
Modal analysis
Sensitivity analysis
Laser Doppler Vibrometry

ABSTRACT

Investigating tribological systems using tribometers is challenging due to the complex interaction between machine vibrations and contact forces. Numerical simulations are therefore essential for interpreting tribological measurements and for improving the design and reproducibility of test rigs. To support the analysis of wear patterns by coupling structural dynamics and contact behaviour, this study develops and validates a high-fidelity finite element model of a twin-disc tribometer as the structural-dynamic foundation of a digital twin. The model includes detailed geometry, bolt pretension, nonlinear contact, nonlinear joints and rigid body components to accurately capture the dynamic behaviour of the system. A sensitivity study quantifies the influence of model parameters on the modal system characteristics. Operational modal analysis of vibrometer measurements confirms the numerical model, and enables the identification of vibration modes that strongly modulate the disc contact forces. These modes are shown to be governed primarily by disc cover stiffness, contact friction and bearing stiffness, explaining experimentally observed shifts in resonance frequencies associated with periodic wear patterns. The validated model therefore provides insights into the interaction between machine dynamics and contact behaviour and forms a basis for the development of a digital twin, taking machine dynamic effects into account.

1. Introduction

The tribological phenomena of friction, wear and lubrication play a crucial role in the performance, durability and efficiency of mechanical systems in a wide range of industries. Understanding and controlling these interactions is essential for improving energy efficiency, reducing material wear and extending the service life of components [1]. To study tribological phenomena experimentally under defined conditions, tribometers, which are specialised test rigs, are widely used [2]. However, complex interactions between machine dynamics and contact forces often challenge the accuracy and reproducibility of tribological experiments [3]. Since the dynamic behaviour of the experimental setup can significantly affect measured friction and wear, characterising system dynamics is essential for reliable interpretation of tribological results [4].

Considering the high customisation and complex dynamics of tribometers, a simulation-based methodology to assess and predict their behaviour during the design process is highly desirable [5]. This paper therefore presents a workflow for physically modelling tribometers using the finite element (FE) method. A modal FE model of a tribometer captures the inherent dynamics and is tuned and validated using 3D Scanning Laser Doppler Vibrometer (3D-SLDV) measurements. A particular focus is on modal contact forces and sensitivity analyses to understand the influence of specific structural components and model parameters on the tribological contact.

A reduced modal representation of the FE model will serve as the foundation for a multi-body system (MBS) model with an application-dependent contact model in the future, forming a digital twin that supports targeted process and design adjustments. A feasibility study [6] indicates a promising methodology that will be further formalised and developed in the future. The proposed workflow is demonstrated on a twin-disc tribometer as a representative use case.

Twin-disc tribometers are commonly used to study wheel–rail contacts and other rolling–sliding interfaces, enabling detailed analysis of contact mechanics and material behaviour, including slippage, creep,

* Corresponding author at: Institute for Engineering Design and Product Development, TU Wien, Lehárgasse 6 – Objekt 7, Wien, 1060, Austria.
E-mail address: stefan.j.eder@tuwien.ac.at (S.J. Eder).

https://doi.org/10.1016/j.triboint.2026.111778
Received 5 December 2025; Received in revised form 15 January 2026; Accepted 29 January 2026
Available online 3 February 2026

and plastic deformation phenomena [7–9]. They also serve in fatigue and wear investigations of mechanical components, including the characterisation of contact fatigue in gear materials [10] and the assessment of wear behaviour and lifetime prediction methods for polymer gears [11].

From an industrial perspective, the motivating use case is soft-nip calendering in paper production, where a polymer-covered roll can develop *barring* or *chatter marks*, which are periodic, polygonal wear patterns along the roll circumference. Barring arises from self-excited vibrations caused by process–structure coupling and uneven wear within the roll stack. Once initiated, these vibrations can quickly amplify, degrading paper quality, increasing noise, and accelerating roll damage, leading to costly downtime. Understanding and predicting the machine dynamics that cause barring is therefore central to model-based design and monitoring [12].

In this work, the twin-disc tribometer serves as a controlled model system to investigate the mechanisms underlying barring, with the FE model focusing on the components and parameters most relevant to its onset.

Prior work provides experimental and numerical evidence that machine dynamics govern the onset and growth of barring. Puhwein et al. [13] analysed barring and the dynamics of the twin-disc tribometer using 3D-SLDV measurements and identified rotational excitation, damping behaviour, and slip-induced stresses as dominant contributors to damage growth, indicating that a more detailed analysis around ~1230 Hz is required. Complementary mechanical modelling by Wiendl [12] explains two instability causes in calenders (sudden vibrations at high speed and gradual barring over days to weeks) and shows how one-sided coupling in the roll-web contact can produce self-excited vibrations. To further expand upon these findings, Peesapati et al. [14] demonstrated that chatter occurrence can be detected using experimental vibration data and machine learning methods, achieving high prediction accuracy but providing limited physical insight for design countermeasures. These studies highlight the strong coupling between structural dynamics and tribological response, underlining the need for predictive models that integrate both aspects.

The correlation of Finite Element Analysis (FEA) with 3D-SLDV measurements is commonly used to model and predict the dynamic behaviour of mechanical systems [15–17]. Although the technique is well established, its application to tribometers is still emerging and poses challenges such as the need for sophisticated model update procedures and line-of-sight constraints to contact zones [15,18].

Against this background, it is important to take a look at how the structural dynamics of tribometers have been studied to date. Previous studies have investigated the dynamics of tribometers either through experimental modal analysis [19] or modelling of local contact interfaces [20,21]. A study has addressed friction-induced vibration and barring phenomena by combining a FE contact model with a simplified representation of the supporting structure (i.e. lumped-mass spring–damper systems) [22]. A structural FE model has been reported for a simplified pad-on-disc configuration in the context of reduced order models and investigation of vibration instabilities [6].

However, these approaches either do not resolve the full structural dynamics of the test rig under operating preload conditions and therefore consider only local nonlinearities, or they lack extensive experimental validation of spatially resolved vibration mode shapes that directly modulate contact forces. As a result, the role of machine dynamics in governing periodic wear phenomena such as barring remains insufficiently understood at the level of the complete test rig.

In the present work, we address this gap by developing and experimentally validating a comprehensive FE model of an entire twin-disc tribometer, incorporating detailed geometry, bolt pretension, nonlinear contacts, nonlinear joints and rigid body components. The main contributions are (i) a nonlinear full-system modelling strategy enabling sensitivity analysis of the dynamic response with respect to key design and operating parameters, (ii) a contact-force-based mode selection criterion linking structural modes to tribological relevance, (iii) a frequency response function (FRF) based mode tracking and updating workflow robust to mode crossing, and (iv) experimental validation using multiple 3D-SLDV configurations. Unlike prior studies, in which structural nonlinearities are either neglected or introduced in isolation, the proposed approach integrates multiple preload-dependent nonlinearities at the system level within a single validated framework. Due to substantial differences in geometry, boundary conditions, and operating preload among existing tribometer studies, the benefit of the proposed integrated nonlinear modelling approach is demonstrated through quantitative validation against experimental measurements of the same physical system. This workflow enables the identification of machine-dynamic mechanisms governing resonance shifts associated with barring, thereby explicitly linking structural dynamics to tribological wear phenomena and improving the physical interpretation of tribological test results.

All modelling and simulation tasks are performed using ANSYS Workbench 2024 R2 [23], while Polytec's PSV Software [24] and MATLAB R2024b [25] are used for experimental data evaluation and 3D-SLDV/FEA correlation.

2. Method

2.1. Use case: Twin-disc tribometer

The investigated twin-disc tribometer, shown in Fig. 1, consists of two independently driven axes 1 and 2, each capable of carrying discs of different diameters. In the current application, disc 1 (diameter $d_1 = 145$ mm) with an fibre-reinforced composite cover is pressed against the steel disc 2 (diameter $d_2 = 145$ mm) in order to model the tribological contact during a calendering process in the paper industry. The independent control of angular velocities ω_1 and ω_2 allows for the adjustment of sliding–rolling ratio (SRR), defined as

$$SRR = \frac{2\,(v_1 - v_2)}{v_1 + v_2} \tag{1}$$

from 0.5% up to 200% at circumferential speeds v_1 and v_2 of approximately 4 m/s. Each axis includes a servomotor, a torque-measuring shaft, and a bearing housing. Axis 1 is fixed to a sliding table, which is supported by eight air bearings in the YZ-plane. Magnets pretension the air bearings in Y-direction and prevent the sliding table from lifting off. The air bearings allow a low-friction motion in X-direction and thus the static force F_N of the pneumatic cylinder is directly transferred to the disc contact. This pneumatic cylinder is attached to a spindle drive to allow adjustment for different disc diameters. To reduce vibrations during operation, a rubber bumper is positioned between the pneumatic cylinder and the force arm. A load cell measures the adjustable normal force applied on the sliding axis during operation. Axis 2 is fixed to an aluminium profile frame. Fig. 1(a) illustrates the entire twin-disc tribometer, Fig. 1(b) shows a detailed view of the tables, axes, discs and housings, which is called *drive train* in the following sections.

2.2. Workflow of the modelling and validation process

While traditional model updating is well established [15,16], there are many challenges in a real-world system such as this tribometer, and therefore a novel workflow has been developed. Fig. 2 provides a schematic overview of the modelling and validation steps.

The methodology expands upon the standard practice of creating a reference model followed by a model reduction for sensitivity analysis. Since the model is rather large and a broad frequency spectrum (100–1500 Hz) is considered, experience has shown that standard tools for automatic model updating in combination with rigid body components, point masses and contact conditions often cause stability or runtime problems. To prevent such difficulties, key novelties used in this study are the integrated treatment of nonlinearities within a

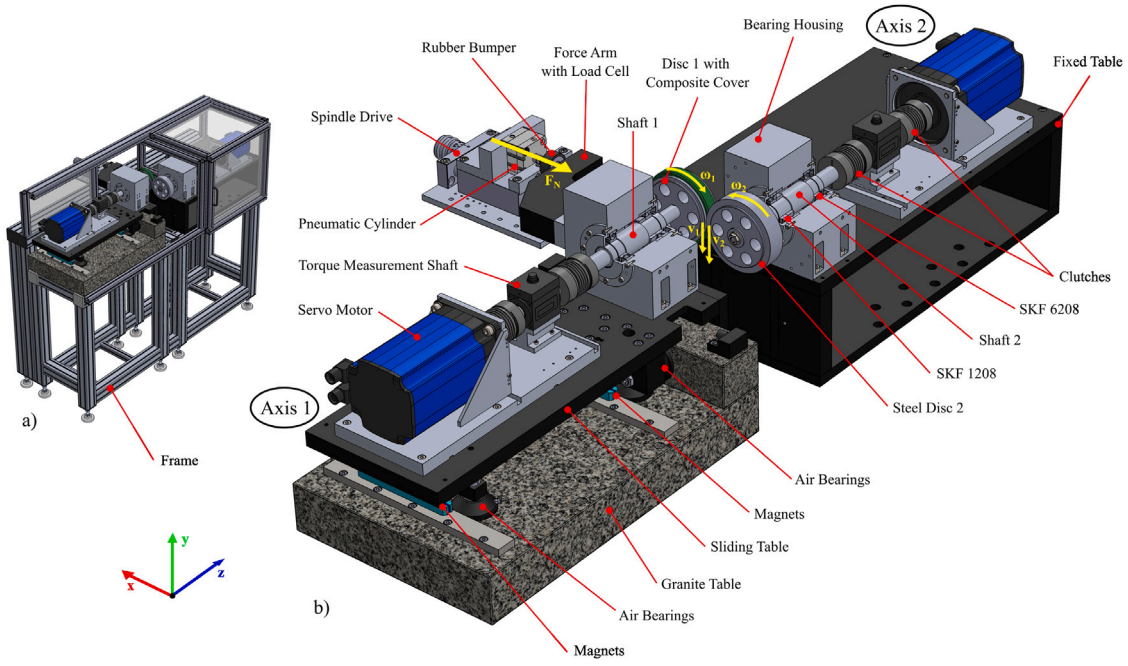

Fig. 1. Overview of the components in the investigated twin-disc tribometer. (a) Geometry model which is used for finite element simulation. (b) Enlarged view of the assembly without the frame, with the bearing housings cut open for better visualisation of the components. The frame measures approximately 650 × 1450 × 1700 mm and each disc has a diameter of 145 mm.

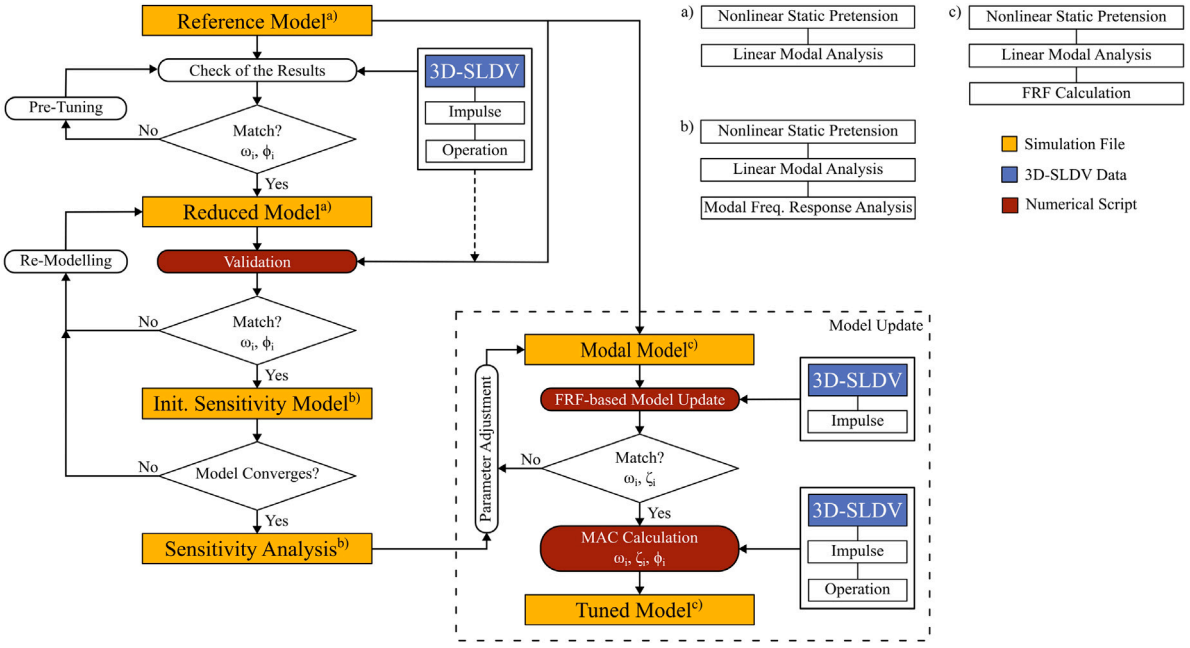

Fig. 2. Workflow of the simulation and validation process. A detailed and finely meshed reference model is first compared against 3D-SLDV measurements using impulse and operational excitation. A reduced model is then derived for efficient sensitivity analysis, enabling identification of parameters governing tribologically relevant vibration modes. Based on these results, a modal model is updated using frequency response functions and correlated with 3D-SLDV data, yielding a validated, tuned model. ω_i, ϕ_i and ζ_i denote the natural frequencies, mode shapes and damping ratios of mode i.

sensitivity analysis (see Section 2.3.4), the FRF-based model updating process (see Sections 2.3.3 and 2.3.5) and the automated eigenvector comparison (see Section 2.5).

The workflow for modelling and validation includes several stages. First, a detailed nonlinear reference model (see Section 2.3.1) is built, incorporating nonlinear contacts, bolt pretension, nonlinear joints and rigid body components. The model is used to perform a linear modal analysis at a statically preloaded state.

In an initial validation step (see Section 3.1), the mode shapes and natural frequencies of the reference model are compared to those obtained from the 3D-SLDV measurements (see Section 2.4). The 3D-SLDV measurements include data obtained from both operational excitation

and controlled impulse hammer excitations. Modal parameters are extracted using an Operational Modal Analysis (OMA) algorithm based on stochastic subspace identification (SSI) [26].

To allow for efficient parametric studies, the reference model is then optimised, rendering a reduced model (see Section 3.2) suitable for a sensitivity analysis. In a preliminary configuration with nominal parameters assigned, this reduced model is used for evaluating model convergence robustness (initial sensitivity model).

A sensitivity analysis (see Section 2.3.4) is conducted using ANSYS optiSLang [23] to quantify the influence of empirically estimated parameters and nonlinearities. Modes are tracked through FRF peaks of characteristic geometric features to overcome the challenge of mode crossing (see Section 2.3.3).

Finally, the reference model is tuned according to the sensitivity analysis results (see Section 3.3) by aligning FRFs (see Sections 2.3.5 and 3.4) and mode shapes (see Section 3.5) with experimental data obtained from 3D-SLDV measurements. The damping parameters are also estimated in this step. The proposed process is described in the respective sections below.

2.3. Finite element models and analysis types

To achieve a high degree of model verification during the model development phase, the FE model is created following the V-Model for mechatronic system design defined in VDI 2206 [27]. Accordingly, the tribometer is first divided into sub-assemblies and further into individual components. Each sub-model is analysed and validated using manufacturer data such as stiffness, mass, inertia and natural frequency. The verified sub-models are then re-assembled and simulated stepwise, enabling plausibility checks, mesh convergence analyses, and numerical convergence tests at each hierarchy level. This structured top-down/bottom-up procedure ensures traceability and consistency throughout the model verification process.

2.3.1. Nonlinear static pretension

Nonlinear system identification is a central topic in structural dynamics and a purely linear modelling approach often fails to predict the complex dynamic behaviour accurately [28,29]. The investigated tribometer contains a large number of nonlinearities that cannot be neglected in the modelling process. These include nonlinear contacts, i.e. the disc contact and the contacts of the bolted connections. Although the contact force is approximately linearly proportional to the indentation depth when Hertz's contact theory for cylinders with parallel axes is assumed [30], the contact area increases with increasing contact force. When modelling frictional contacts, this effect, which is also a geometric nonlinearity, must be taken into account in order to be able to correctly estimate the contact stiffness in a modal analysis. The same applies to the frictional contact surfaces in bolted connections, where the number of sticking contact elements in the FE model affects the modal behaviour [31]. The system also contains nonlinear elasticities, such as rolling bearings, air bearings, elastomers and a pneumatic cylinder, whose stiffnesses are influenced by the preload. To consider these nonlinearities in the FE models, a nonlinear static pretension analysis is initially performed for each model, with an operational normal force of 800 N before linearisation (see Section 2.3.2) [31]. This approach allows model refinement based on 3D-SLDV measurements and follows similar principles to the structured methodologies proposed in [32,33], where nonlinearities are identified and integrated into FE models via staged identification and validation processes.

The resulting modal parameters are sensitive to the selected operating point, as the preload directly affects contact-relevant modes through the nonlinear elements, which is shown in Section 3.3. A significantly lower preload level, down to the point of zero normal contact force, would therefore result in a different dynamic system and altered modal results. However, investigating significantly different preload levels would constitute a strong extrapolation of the validated model and is therefore not pursued here, as the experimental validation is available only for the nominal preload level of 800 N. Nevertheless the preload sensitivity is captured locally within its measured fluctuation range (see Table 2).

As a result, the present model is limited to predicting vibrations around the statically preloaded operating point and does not capture transient effects associated with evolving contact conditions. Such effects are intended to be addressed in future work by coupling the validated structural model to a transient MBS model within a digital twin framework.

Geometry Model: Pre-processing initially involves the preparation of the geometry model shown in Fig. 1 to enable efficient meshing of the FE model. During this step, components irrelevant to the calculation, such as pneumatic tubes, are removed. To ensure a high level of physical detail, the bolted connections are also incorporated into the geometry model, however to simplify meshing, these bolts are represented by cylindrical bodies. To capture low-frequency modes and frame movements, the frame is modelled as an equivalent beam structure.

Materials and Stiffness Behaviour: An overview of the assigned materials is given in Fig. 3(a) and the stiffness behaviour is provided in Fig. 3(b). ANSYS standard materials Aluminium Alloy and Structural Steel are assigned to components assumed to behave linear elastically. The beam model material parameters are tuned to match the high-fidelity frame model response.

For purchased components (i.e. spindle table, granite table, servomotors, torque measurement shafts, and couplings), detailed internal geometry and material data required for flexible modelling are not available. Where manufacturer specifications provide only global dynamic properties (mass, inertia, stiffness or characteristic frequencies), these components are represented as rigid bodies with equivalent properties. This approach avoids introducing poorly constrained flexible models and is justified as their internal structural modes are not expected to dominate the contact-relevant frequency range investigated. The assumption is additionally supported by the good agreement between simulated and measured system responses shown later on in Section 3.4.

While fibre-reinforced polymers may exhibit nonlinear behaviour, detailed nonlinear material data is not available. In the disc cover, the fibre-reinforcement is predominantly oriented in the circumferential direction. Therefore, the stiffness in the contact normal direction is primarily determined by the matrix-dominated behaviour in radial direction. For modal analysis the cover is therefore represented by an effective linear elastic isotropic modulus of elasticity calibrated at the operating point.

For modal analysis, the quantity of interest is the effective stiffness corresponding to the preloaded operating point. Accordingly, the sensitivity analysis varies the disc cover Young's modulus within empirically determined average bounds to assess its influence on tribologically relevant modes, see Section 2.3.4. This effectively represents changes in preload-state stiffness that would also arise from nonlinear material behaviour. As shown in Section 3.4 this approach allows the experimentally observed resonance shifts to be reproduced without introducing poorly constrained material models.

Sub-Assembly Interfaces: Next, boundary conditions, including contacts and constraints between components, are specified. For the contact interfaces of the bolted connections, a frictional contact with a static coefficient of friction (CoF) of $\mu_s = 0.15$ is assumed. The contact behaviour allows sliding and separation. Initially, it is assumed that the contact surfaces only touch each other without penetration. To simplify modelling, the connections between the bolt heads and the interacting components are treated as a bonded contact. The preload of the bolts is introduced by applying axial forces to the bolt shafts. The applied preload force is calculated according to VDI 2230, a standard reference work for calculating bolted connections [34].

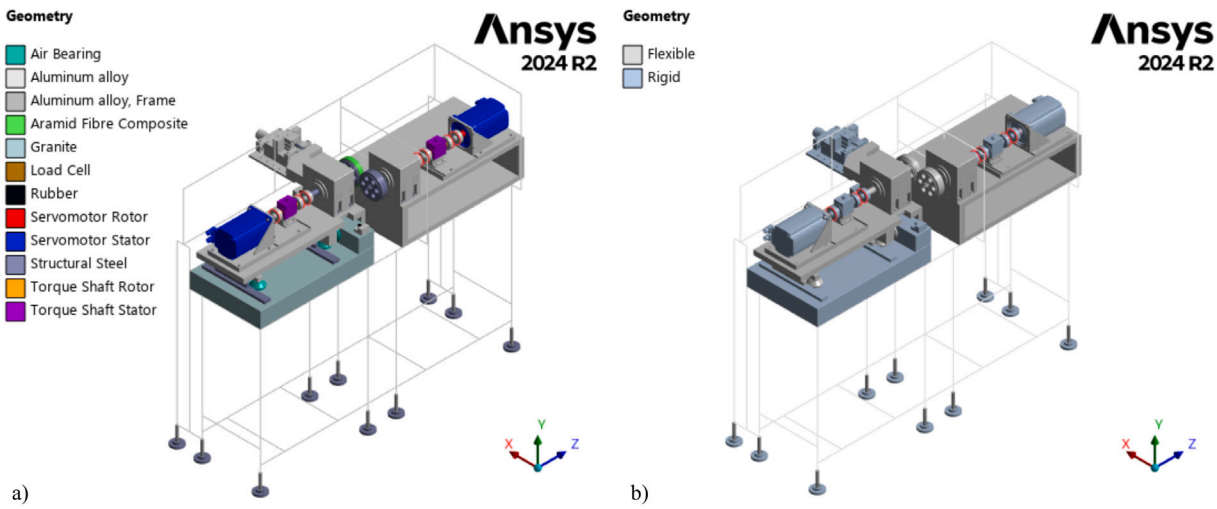

Fig. 3. Finite element model (a) assigned materials (b) flexible and rigid bodies.

The contact between the discs is initially defined as frictional, with $\mu_s = 0.1$, based on an average measured CoF from experiments. A Lagrange multiplier method is used to formulate the disc contact and ensures that a gap may be present but no penetration is allowed [35, 36].

In the present study, the CoF is treated as an effective constant parameter. This is consistent with the linearised modal analysis, which represents the system behaviour around a statically preloaded operating point. While velocity- and temperature-dependent friction effects may influence transient contact behaviour, their impact on the tangent stiffness governing the identified modal properties is approximated through the sensitivity analysis of the friction coefficient.

As previously mentioned, the couplings and torque measurement shafts are modelled as rigid bodies connected by elastic joints. The complex geometry of the couplings is reduced to a bushing with 6 degrees of freedom (DoF), with elastic properties defined by data sheet specifications. To account for the total mass and moments of inertia, additional point masses are defined within the separated coupling half-shells. The dynamic properties of the couplings can be validated against the manufacturer's specifications in isolated sub-models. A similar approach is applied to the torque measurement shafts. However, in this case the shaft is assumed to be rigid in radial direction and thus only the rotational stiffness is selected according to the manufacturer's specifications.

The bearing locations of the two main shafts, which support the discs, are also modelled using bushings. Each of the two bearing housings contains a SKF 1208 and a SKF 6208 ball bearing. The nonlinear stiffness characteristics of these bearings are determined using the *SKF SimPro Quick* software [37] and cross-checked using the ANSYS Add-In *SKF Bearing App* [38]. The translational stiffnesses are implemented within the bushings as nonlinear force–displacement curves.

The rubber bumper and the pneumatic cylinder are replaced by linear elastic springs. The linear stiffness of the rubber bumper c_{RB} is estimated for the reference model and varied in the sensitivity analysis using an equivalent cross section A, Young's modulus E and the bumper length l

$$c_{RB} = \frac{EA}{l}. \tag{2}$$

Since rubber exhibits strong frequency-dependent behaviour, Koblar & Boltežar [39] experimentally measured the dynamic Young's modulus of rubbers with Shore 40 A and 63 A hardness. Given the rubber bumper in the tribometer with a Shore hardness of 57 A, a representative modulus between 15 MPa and 30 MPa is chosen based on the measured dynamic behaviour of similar rubbers.

Table 1
Overview of the load steps for each nonlinear static pretension analysis.

Boundary condition	Load Step 1	Load Step 2	Load Step 3
Bolt pretension	Load	Lock	Lock
Preload force application	Deactivated	Load	Lock
Translational DoF spindle table	Open	Open	Lock

To estimate the pneumatic cylinder stiffness, an isothermal change of state is assumed for small displacements of the cylinder. Assuming an initial pressure p and a volume V the ideal gas equation renders

$$pV = p\,Al = Fl = mR_sT\,, \tag{3}$$

for a cylinder with cross section A of length l under the assumption of constant mass m, specific gas constant for dry air R_S and temperature T. For constant temperature the cylinder force $F(l)$ becomes

$$F(l) = \frac{mR_sT}{l} \tag{4}$$

rendering the approximated stiffness

$$\frac{dF(l)}{dl} = -\frac{mR_sT}{l^2}. \tag{5}$$

The underlying assumptions for the calculation are highly simplified. The nonlinearity of the stiffness is not explicitly captured, but linearised for the purpose of sensitivity analysis. Accordingly, the Taylor expansion is centred on a nominal operating point for which a linear approximation appears sufficient.

Meshing: Only 10-node tetrahedron and 20-node hexahedron elements with quadratic shape functions are used. Mesh convergence is checked in two iterations using the reference model. The mesh size of the components is reduced by around 30% in each iteration. After the second iteration, all 400 extracted modes have a frequency deviation of <1%. The mesh is therefore regarded as converged with respect to the modal analysis. A dedicated convergence study is carried out for the meshing of the disc contact.

Boundary Conditions: The boundary conditions are applied in three load steps, shown in Table 1. Load step 1 includes the pretension of all bolted connections. In load step 2, the system is preloaded by a joint force of the translational joint in the spindle table. In the third load step, the translational DoF of the spindle table is locked to prevent it from sliding during the modal analysis.

The final reference model shown in Fig. 3 contains a total of 256 bodies, including 36 rigid bodies, 182 linear contacts, 23 nonlinear contacts, 58 joints, 10 beams and 2 springs.

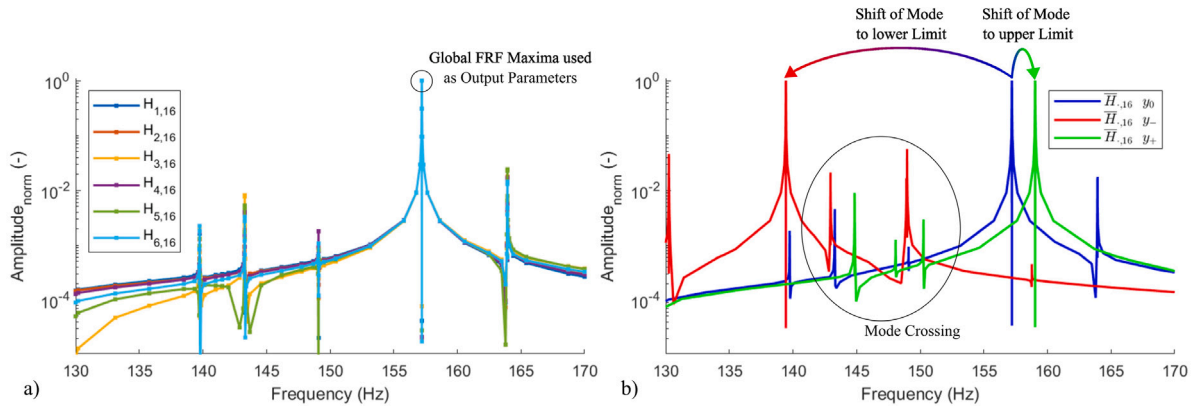

Fig. 4. (a) Frequency response functions of the six geometric criteria $H_{k,16}$ of mode 16. (b) Shift of the averaged FRF $\overline{H}_{.16}$ resonance peaks for parameter variations, where y_- is the lower parameter boundary, y_0 the initial configuration and y_+ the upper parameter boundary.

2.3.2. Linear modal analysis

In ANSYS Workbench the results of the nonlinear static pretension analysis can be used as input for the modal analysis, to linearise a model at an operating point. The true contact status of the nonlinear static analysis after the last load step is used for linearisation, where adhering contact elements are defined as bonded contact, and sliding areas are defined as frictionless contacts without separation [31].

In the reference model 400 modes are calculated to capture all relevant dynamic effects in the considered frequency range up to 1500 Hz. The resulting force reaction of the frictional disc contact is evaluated in order to compare the consistency of the results between the reference model and the reduced model on the one hand, and on the other hand the contact forces serve as a criterion for selecting tribologically relevant modes for the sensitivity analysis.

2.3.3. Modal frequency response analysis

The parameter variations can result in strong changes in the natural frequencies of certain modes, which are typically sorted for ascending natural frequencies. During parameter variation *mode crossing* makes consistent tracking across simulations difficult [40]. In order to be able to track the modes without complex scripting, a workaround is selected via a modal frequency response analysis [41], where the model is excited in the normal force direction of the disc contact with a 100 N force sweep to compute the FRFs.

Mode Crossing: In contrast to the natural frequency the mode shape is a characteristic and unique criterion for tracking a specific mode. Instead of using the entire mode shape vector, whose size is proportional to the DoF of the entire FE model, a simplified approach is suggested for automated tracking using commercial FEM tools. From the eigenvector, 31 geometric criteria C_k are selected, including points, edges, surfaces, and rigid body elements (i.e. mass points). The FRF H_k is calculated for each C_k and averaged over all mesh nodes in the case of edge- or surface-based criteria. For each mode i, those criteria $C_{k,i}$ are selected whose dynamic response clearly reflects the corresponding mode shape. The FRFs $H_{k,i}$ are computed for each mode and the global maximum is identified within the frequency range of interest. The corresponding frequency is used as an output parameter in the subsequent sensitivity analysis, where the correlation coefficient is computed to quantify the sensitivity of the mode's natural frequency to variations in the model's input parameters. Fig. 4(a) shows an example of the FRFs $H_{k,16}$ obtained from six geometric criteria of mode 16.

Fig. 4(b) illustrates the shift of the FRF maxima from the lower parameter boundary y_- to the upper boundary y_+, with respect to the initial configuration y_0, given in Table 2. The FRF maximum identifies the tracked mode, even in cases where natural frequencies cross (see Section 3.3).

Force Criterion: The modes for the sensitivity analysis and subsequently for the reduced modal model are selected from the reference model based on the resulting total force in the disc contact. If the force exceeds the threshold value of 30% of the maximum force as shown in Fig. 5, the mode is selected for further analysis. This value is chosen in order to select sufficient modes for a sensitivity analysis while significantly reducing the model. Since the numerical simulation renders a strong increase in force amplitude at around 700 Hz, the threshold is set separately below and above this frequency limit. For each frequency range, the dominating modes with the highest interaction forces are selected, rendering 16 representative modes for the sensitivity analysis.

2.3.4. Sensitivity analysis

Table 2 lists the parameters varied in the sensitivity analysis. In the initial sensitivity model, the stability of the previously described output parameters and the convergence of the model within the parameter limits are tested. The parameter limits are based on experimental data and manufacturer specifications.

A preliminary selection of relevant input parameters is carried out based on engineering knowledge, potential impact on the system dynamics and efficient implementation in the FEM tool. This screening indicates that the chosen parameters combine high expected influence with robust parametrisation, while several further candidates (e.g. peripheral masses, cables, magnet forces) are either poorly constrained or are not expected to affect resonance locations and natural frequencies within the investigated frequency range and were therefore omitted.

Contact compliance effects are addressed through dedicated mesh and contact convergence studies, while variations in effective tangential and normal contact stiffness are further captured through sensitivity analysis of the friction coefficient and the disc cover Young's modulus.

Structural damping is included in the subsequent model updating steps (see Section 3.4) since it affects the amplitude and bandwidth of the frequency response but hardly affects the natural frequencies themselves.

Bolt pretension is treated as a fixed assembly condition rather than an uncertainty parameter. Variations in bolt preload would represent different assembly states and are therefore not considered within the sensitivity analysis of the validated configuration.

As the bearing stiffnesses are defined as nonlinear stiffness curves, their nonlinearity is mapped by varying the preload. The Z-position of the disc cover is varied in three discrete steps to enable a robust update of the geometry model. In the course of the sensitivity analysis, 304 parameter configurations were automatically calculated. Since each parameter configuration includes the calculation of the nonlinear static pretension, the linear modal analysis and the modal frequency response analysis, the computational costs are quite high.

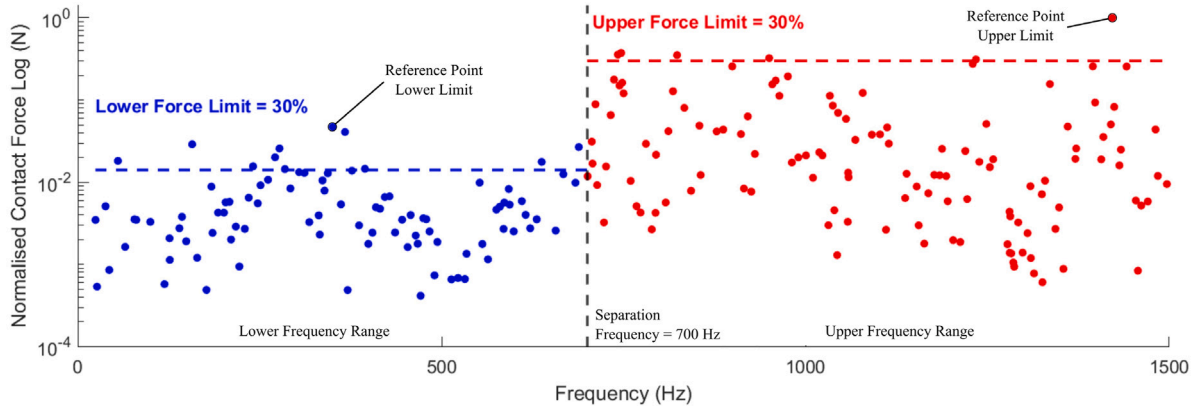

Fig. 5. Normalised forces of the disc contact for each mode of the reference model. A 30% threshold of the maximum contact force is applied separately below and above 700 Hz to account for the force increase near this frequency. Modes whose disc contact forces exceed the threshold are selected for sensitivity analysis.

Table 2
Overview of the parameters analysed in the sensitivity study for the lower boundary y_-, the initial values y_0 and the upper boundary y_+.

Input parameter	Symbol	Boundaries			Unit	Discretisation
		y_-	y_0	y_+		
Pretension force	F_N	700	800	900	N	Continuous
Young's modulus composite	E_{DC}	3000	5000	7000	MPa	Continuous
Disc position Z	u_Z	−1	0	1	mm	$u_Z \in \{-1, 0, 1\}$
Disc contact CoF	CoF	0.05	0.10	0.15	–	Continuous
Stiffness pneumatic cylinder	c_{PC}	80	100	120	N/mm	Continuous
Stiffness rubber bumper	c_{RB}	1475	2213	2950	N/mm	Continuous
Stiffness air bearing	c_{AB}	150	346	350	kN/mm	Continuous

2.3.5. Modal model and comparison of frequency response functions

For model reduction, the modes relevant to the structural response must be identified. Since the contact behaviour is dominated by the disc dynamics, particular focus is on accurately capturing the modal response of the discs. In addition to numerical force evaluation (see Section 2.3.3) experimental validation is carried out using impulse hammer tests. Fig. 6(a) shows the test setup and typical FRFs. The impulse hammer excitation is applied in the contact normal direction, the response is measured at a point on the steel disc in X-, Y- and Z-direction. These measurements were performed for 12 different disc covers, where each cover is measured in 12 angular positions over the circumference.

In order to compare the measured FRFs with the response of the simulation, the reference model is excited and the mobility transfer function is calculated using the NVH Tool [41]. As the force excitation point of the impulse hammer varies slightly when changing discs, the FE model captures this effect by exciting 7 points close to the excitation point (see Fig. 6(b)). The response is calculated for each excitation point at the location of the 3D-SLDV measurement. Based on the 12 measured positions per disc and the 7 excitation points, the statistical properties mean value μ and standard deviation σ can be computed. The FRF comparison of measurement and simulation (see Section 3.4) allows in combination with the force criterion (see Fig. 5) the identification of those modes (from over 400 available) that significantly contribute to the measured structural response of the disc. These selected modes form the modal model, which is a reduced representation of the full FE model. The FRF comparison also enables the natural frequencies of the modal model to be tuned based on the results of the sensitivity analysis and a constant modal damping ratio is assigned to each identified mode.

2.4. Vibrometer measurements and data evaluation

The test setup described in [19] is used to capture the tribometer dynamics. It consists of a 3D-SLDV and a single beam 1D-LDV reference. Measurements are performed across a custom grid, capturing vibrations up to 25 kHz. An extensive measurement campaign was carried out at the twin-disc tribometer in various configurations and three spatial directions. The measurements in five different configurations covered multiple components, see Fig. 7.

The measurement positions were determined by the space available in the laboratory. The tribometer was excited both by operating conditions and by controlled impulse hammer excitation. The operational measurements were carried out with and without slippage between the discs. Without slip ($SRR = 0\%$), both axes were operated at 526.8 rpm (~8.78 Hz). To obtain slip for the second measurement campaign, the rotational speed of the second axis was increased to 539 rpm (~8.98 Hz), resulting in $SRR = 2.3\%$.

Since high-frequency modes of the drive train, which exhibit particularly high dynamic contact forces (see Fig. 5), were not sufficiently excited by the low impulse of the lightweight impulse hammer, operational data was additionally used for identification, to avoid missing weakly excited but tribologically relevant modes. Especially slip operation excites modes across the entire frequency spectrum under consideration and complements impulse hammer tests. In addition, local frequency response functions were obtained by directly exciting the discs with the impulse hammer at a dedicated measurement location, enabling direct comparison between measured and simulated disc responses (see Fig. 6).

All measurements are processed using an SSI-based OMA algorithm, which allows to reliably estimate the mode shapes and the natural frequencies. The robustness of the identified modal parameters was assessed based on repeatability across independent measurement runs, different excitation conditions, and multiple spatial measurement perspectives. Only datasets exhibiting stable operating and contact conditions, well-defined operational deflection shapes, and consistent spectral peaks were retained for model validation, while measurements affected by poor signal quality or non-stationary operating conditions were excluded. In densely populated frequency ranges, increased frequency scatter and the identification of multiple closely related mode

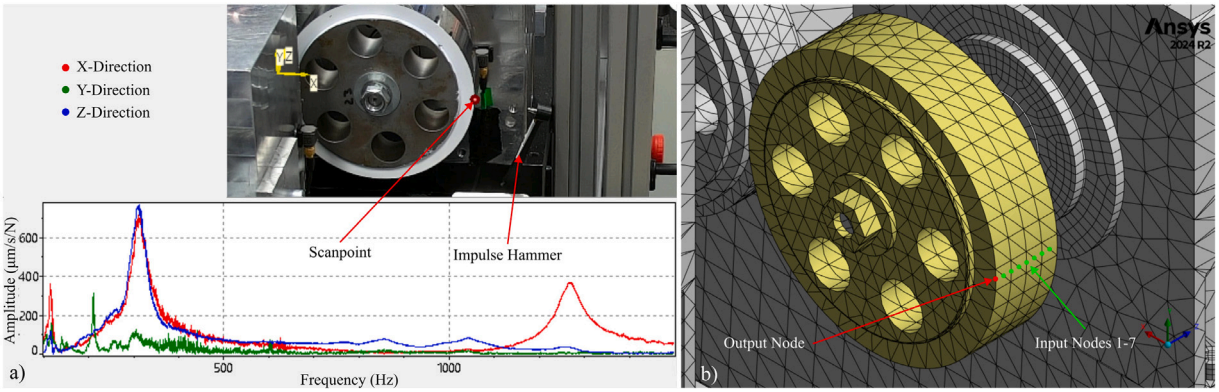

Fig. 6. (a) Evaluation of the impulse hammer measurements on the steel disc in Polytec's PSV Software. The discs were excited in contact normal force direction. (b) Input and output nodes for numerically computing the frequency response.

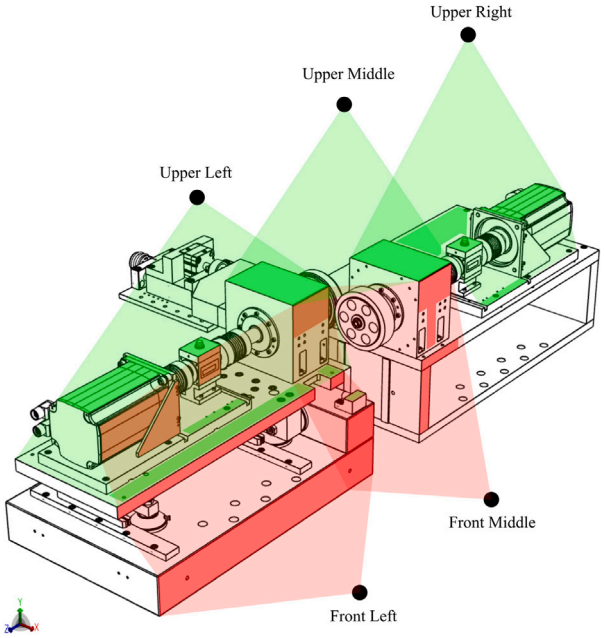

Fig. 7. Schematic representation of the five 3D-SLDV measurement positions and the measured components used in the setup.

shapes were observed. This behaviour reflects known limitations of OMA in the presence of high modal density, measurement noise, and restricted observability due to line-of-sight constraints [42]. Despite these effects, the tribologically relevant modes were consistently identified across the considered measurement configurations, providing a reliable basis for model validation.

The damping parameters are also calculated, but OMA is rather inaccurate, see [43], for damping estimation of nonlinear systems. Therefore, the FRFs analysed in Section 2.3.5 are used to evaluate the damping parameters.

2.5. Mode shape correlation

The last step of model validation is the comparison of the mode shapes ϕ_i from numerical and experimental data, using the modal assurance criterion (MAC) [42,44]. Since the measurements include different 3D-SLDV setups with local reference frames they must be transformed to global coordinates of the simulation model for proper processing. Since mesh nodes and corresponding measurement scanning points do not coincide, the simulation results have to be interpolated at the measurement points. Linear spatial interpolation is used to correlate simulated mesh nodes and scanning points. This procedure is repeated for each measurement point for accurate calculation of the MAC value.

Table 3
Overview of model size, analysis settings and calculation time.

Model	Nodes	Elements	Substeps	Modes	Time (hh:mm:ss)
Reference model	719 289	338 423	9	400	01:03:43
Reduced model	517 353	217 709	3	350	00:20:57
Change	−28.1%	−35.7%	−66.7%	−12.5%	−67.1%

3. Results and discussion

3.1. Pre-tuning: Initial validation of finite element model

Following the workflow described in Fig. 2, the first step is to check the plausibility of the model. Polytec's PSV software is well suited for quickly checking the measurement data. As shown in Fig. 8(a), the response amplitudes can be visualised in the frequency domain for operational excitation and for impulse hammer excitation alternatively as FRF. Although this visualisation does not yet represent a formal identification, eigenmodes are clearly indicated by high amplitudes and a uniform movement of the measurement points in the animation. The measured response at the resonance is compared to the simulated mode shapes to verify if the measured mode is represented in the numerical model. Fig. 8 shows two visually matching modes from the perspective *Upper Left*. Since the frequencies of approximately 116 Hz in the measurement and 125.8 Hz in the simulation only deviate slightly (8%), this mode is considered preliminarily validated.

In addition, the simulated contact forces in the disc contact serve as indicators of the model quality. The high-frequency modes, which are associated with the formation of barring, also exhibit the maximum contact forces in the reference model. This enables the subsequent reduction of the reference model's size.

3.2. Reduced model and validation to reference model

To reduce computational costs for the sensitivity analysis, the reference model is simplified by (a) increasing the mesh size of non-contact components by approximately 30%, (b) limiting the number of modes to 350 and (c) reducing the number of steps during static pretension analysis from three to one. These modifications reduce the computation time for each load case from over one hour to approximately 20 min. An overview of the adjusted model and analysis settings is given in Table 3.

The procedure described in Section 2.5 is used to validate the reduced model against the reference model. Fig. 9(a) shows the MAC

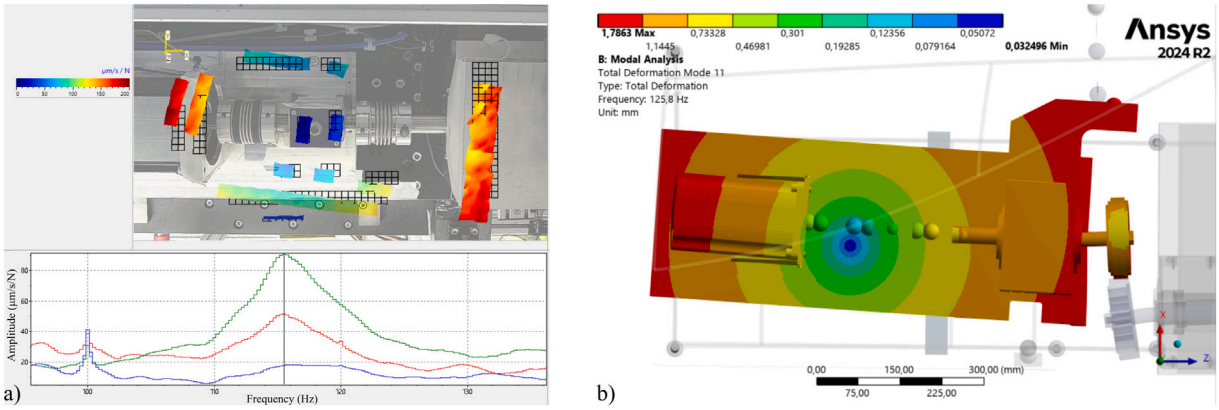

Fig. 8. Two visually matching modes from the perspective *Upper Left*. (a) Mode shape at 116 Hz in Polytec's PSV software with averaged transfer functions. (b) Mode of the reference model at 125.8 Hz, without physical scaling.

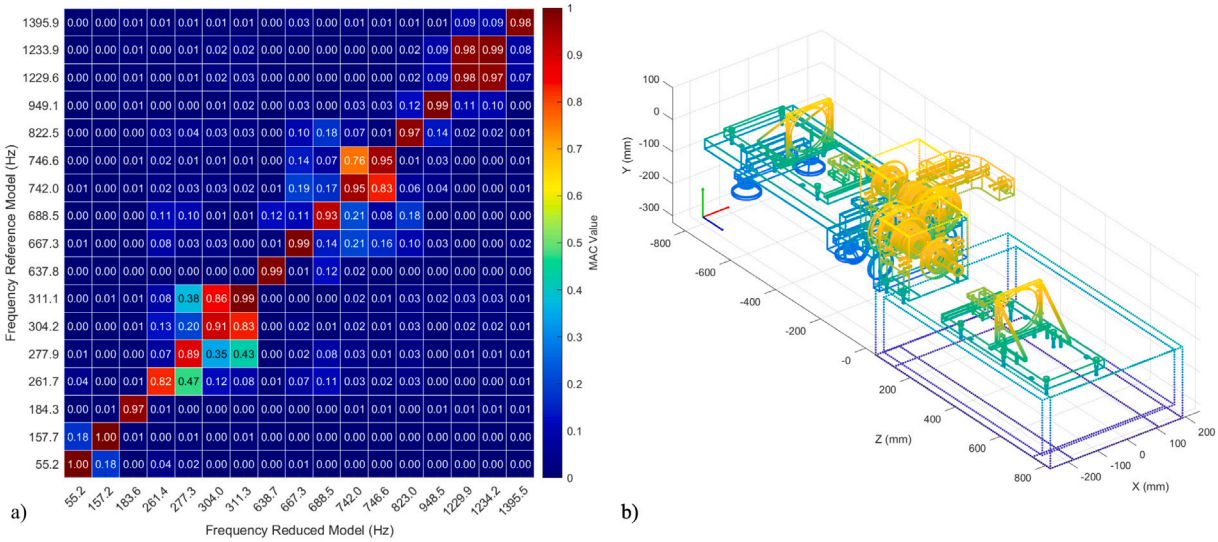

Fig. 9. (a) MAC matrix between reference model and reduced model in the range between 0 Hz and 1500 Hz. The modes are selected by a contact force criterion. (b) Node skeleton of the reduced model used for MAC calculation.

matrix of selected mode pairs up to 1500 Hz. The pairing is based on the disc contact force criterion described in Section 2.3.3, using a deviation threshold of 30% for relative force and 1 Hz for frequency. Modes below and above 700 Hz are again processed separately. Fig. 9(b) illustrates the node skeleton of the reduced model used for MAC calculation. The results of the reference model are interpolated at these nodes.

The cross MAC matrix in Fig. 9(a) indicates a clear match, with a mean diagonal value of 0.96. Given the small frequency deviations and high mode shape correlation, the reduced model is considered validated against the reference model.

3.3. Uncertainty quantification: Sensitivity analysis

In the sensitivity analysis, the correlations between selected parameters (see Table 2) and the natural frequency change of the modal model are evaluated. As described in Section 2.3.3 the mode shape ϕ_i is characterised by several geometric criteria $C_{k,i}$, which can be handled efficiently by commercial FEM tools. Instead of calculating the desired sensitivity in a single step, the partial sensitivities of $C_{k,i}$ are evaluated for each input parameter j before the overall sensitivity can be obtained from statistical properties. Theoretically, all partial sensitivities are identical for properly selected geometric features. However, there might be some outliers which have to be removed before averaging the partial sensitivities to the final results. A partial sensitivity is considered as outlier if its deviation from the mean value exceeds twice the standard deviation. This approach supports robust mode tracking by elimination of inconsistent or unrepresentative criteria during the FRF-based mode tracking (see Section 2.3.3). Fig. 10(a) summarises the outliers per mode and input parameter.

Mode 52 and mode 209 contain most outliers. A possible reason for this is the large number of geometric features (15 and 19, respectively) used for mode tracking. Apparently not all criteria are equally suitable for tracking the mode for all parameter combinations, but after outlier removal the remaining criteria are still statistically reliable. The majority of mode-parameter combinations does not contain any outliers at all.

Fig. 10(b) shows the mean correlation matrix μ_{ij} after outlier elimination. The main factors influencing the natural frequencies can be clearly identified as Young's modulus of the composite disc cover E_{DC}, the friction coefficient CoF in the disc contact and the stiffness of the air bearings c_{AB}. E_{DC} has a significant effect on modes >700 Hz (Modes 103–209), while c_{AB} affects primarily low frequencies <700 Hz (Modes 5–89). On the other hand, CoF appears to affect modes within the entire range.

The pretension force F_N and thus the nonlinearity of the rolling bearing stiffness has a moderate influence on modes in the higher frequency range. Comparing the high rolling bearing stiffness to the air bearings, this correlation seems reasonable. The axial position of

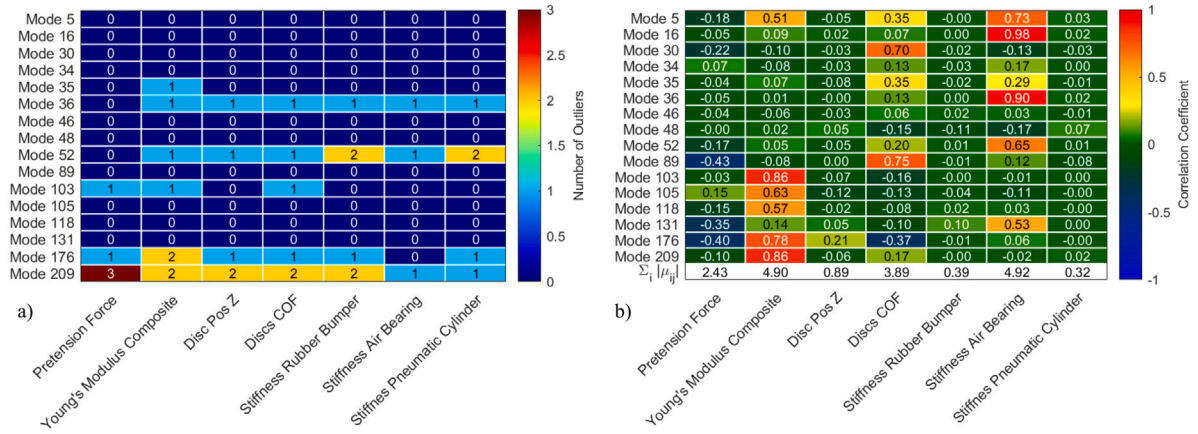

Fig. 10. (a) Number of outliers within partial sensitivities. (b) Averaged correlation matrix μ_{ij} without outliers. The main factors influencing the natural frequencies can be clearly identified as Young's modulus of the composite disc cover E_{DC}, the friction coefficient CoF in the disc contact and the stiffness of the air bearings c_{AB}.

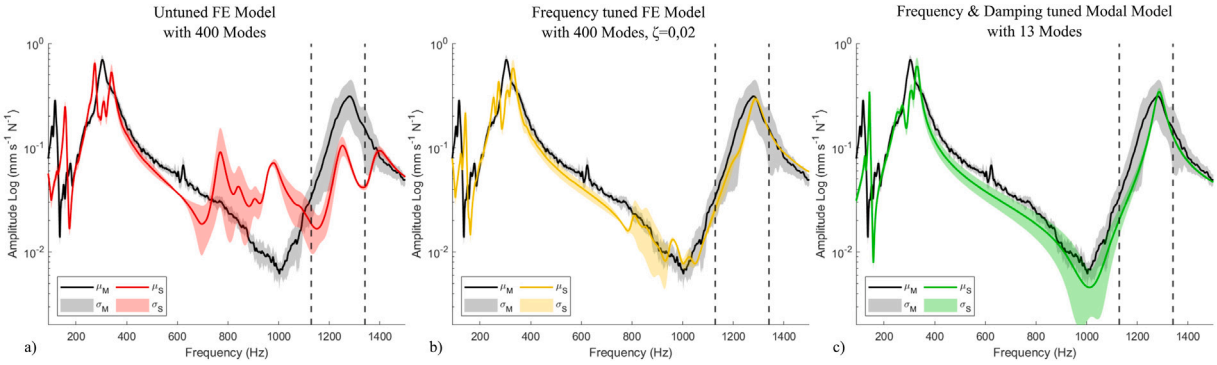

Fig. 11. Model tuning process by comparing the mean frequency response functions of the simulation (μ_S) and the measurement of disc cover 5 (μ_M) with the corresponding standard deviations σ_S and σ_M in X-direction. Colour coding highlights the consecutive tuning steps, while vertical dashed lines indicate the barring-related frequency range. (a) Untuned reference model (b) Reference model after frequency tuning with modal damping $\zeta_i = 0.02$. (c) Modal model with tuned frequencies and modal damping parameters. The tuned modal model shows very good agreement with the measurement.

the composite disc cover u_Z, the stiffness of the pneumatic cylinder c_{PC} and the stiffness of the rubber bumper c_{RB} hardly influence the natural frequencies of the model.

3.4. Model update: Alignment of frequency response functions

Using a parametrised version of the reference model, E_{DC}, CoF and c_{AB} are varied and the FRFs for the nodes indicated in Fig. 6 are calculated. Fig. 11(a) compares the 3D-SLDV measurements for disc cover 5 and the untuned reference model. The statistical properties μ_M and σ_M are visualised for the 12 measured positions per disc, while μ_S and σ_S characterise the simulated results (7 excitation points).

The system response of the FE model after parameter variation is given in Fig. 11(b). In particular, increasing the CoF up to 1 renders good matching in the low amplitude range between 600 Hz and 1000 Hz. Here, the friction coefficient acts as an effective parameter governing the linearised tangential contact stiffness and should not be interpreted as the physical sliding friction coefficient. A detailed investigation of the resonance peak at around 1290 Hz shows that it is also formed by two disc modes. The peak at 152 Hz can be shifted to 140 Hz by reducing the air bearing stiffness to the lower limit, 150 kN/mm.

Finally the damping parameters ζ_i of the modal model (13 modes) are adjusted to match the measurement, see Fig. 11(c). To ensure that all dynamically relevant behaviour is captured, the mode selection is not based on FRF comparison alone. The modes are first preselected using the dynamic contact forces obtained from the FE model (see Fig. 5). From this force-based preselection, those modes that also reproduce the FRF of the full FE model are retained.

As different covers have been tested, E_{DC} is modified next, see Fig. 12. The measurements for different disc covers vary significantly in the 1140 Hz to 1390 Hz frequency range, a behaviour which is also obtained in the simulation, whereas there is a negligible effect for frequencies below 700 Hz. Two effects can be observed in Fig. 12. Firstly, a variation of the high-frequency resonant peak is observed for disc cover 4 and 5 within one disc rotation, which is evident from the increased standard deviation σ_M. This indicates that there is an inhomogeneity in the disc composite cover, which influences the elasticity of the disc.

Secondly, the high-frequency resonance peak is strongly shifted by the disc cover stiffness E_{DC}, an effect which is shown in both, measurements and simulations. Although the disc cover is modelled as a linear elastic material, the actual system behaviour can be mapped qualitatively and quantitatively by varying this parameter. Since experiments show, that the time to barring formation depends strongly on the disc cover used, it can be assumed that this behaviour is mainly influenced by the elasticity of the cover. In addition, the experiments show a directly proportional relationship between the number of chatter marks and the frequency of the resonance peak. The simulation thus provides a direct, quantitative relationship between cover stiffness and the number of chatter marks.

The observed separation of a single resonant peak into two separate peaks (see Fig. 12(a)) with decreasing contact stiffness (Young's modulus) is characteristic for two interacting modes, i.e. a vibration absorber.

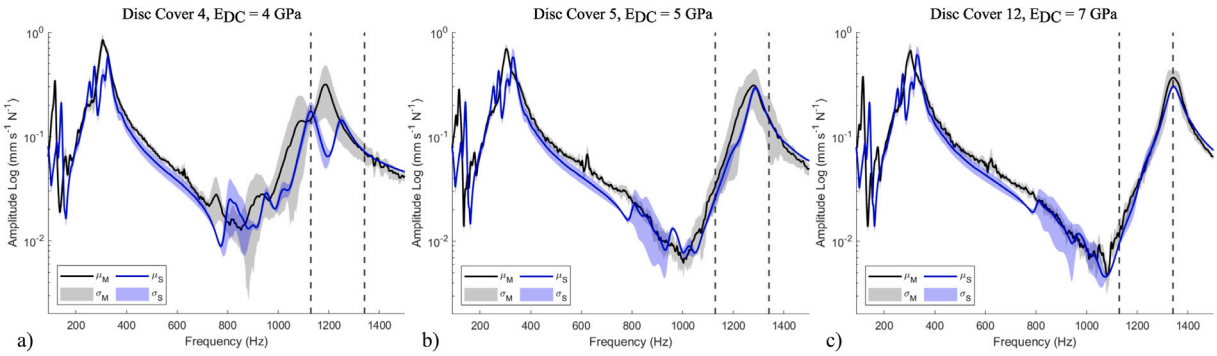

Fig. 12. Comparison of the mean frequency response in X-direction between measurement μ_M and simulation μ_S with the corresponding standard deviations σ_M and σ_S. (a) disc cover 4, $E_{DC} = 4$ GPa, (b) disc cover 5, $E_{DC} = 5$ GPa, (c) disc cover 12, $E_{DC} = 7$ GPa. Frequencies related to barring, indicated by the marked area, are strongly influenced whereas lower frequencies stay nearly unchanged. The numerical FRFs are computed with constant damping of $\zeta = 0.02$.

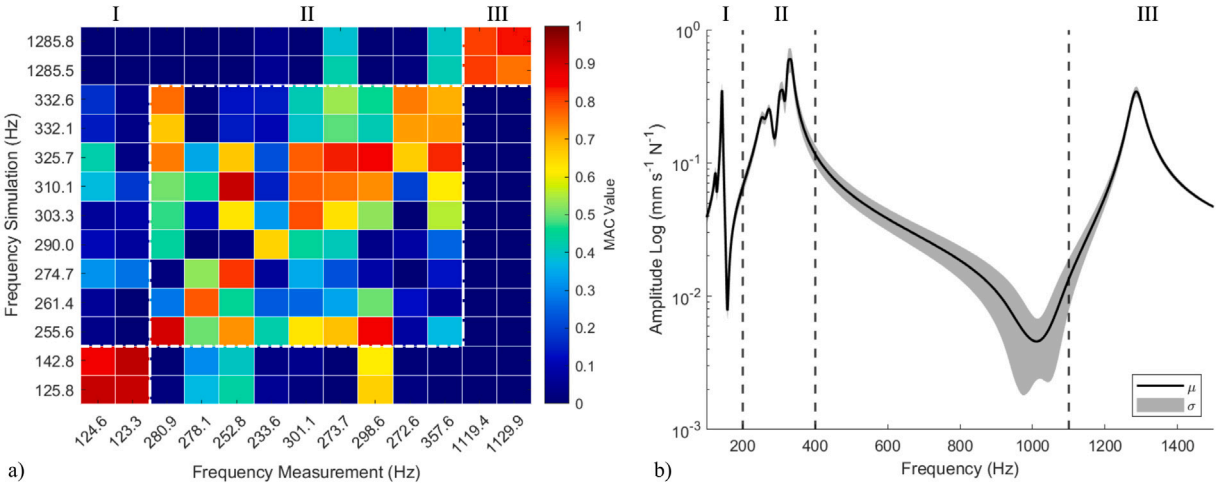

Fig. 13. (a) MAC matrix between 13 simulated modes of the modal model and 13 matched modes from identification. (b) mean simulated frequency response of the modal model. The vertical lines mark the areas I–III of the corresponding MAC matrix. High MAC values in the main diagonal indicate high degree of similarity of measured and calculated mode shapes.

A variation of E_{DC} in the simulation renders FRFs which compare well with the measurements.

3.5. Mode shape validation

In total, 19 different 3D-SLDV measurements with both impulse excitation and operational excitation from different spatial perspectives are used to validate the 13 modes of the reduced order modal model. Unfortunately, the experimental data provided does not allow processing of all the different measurements within a single identification run. Therefore, identifications provide a total of 422 modes which leads to a 13 by 422 MAC matrix. Due to identical measurement positions for both impulse hammer and operational excitation, many redundant modes are identified and represented in the MAC matrix. One possible way to condense the MAC matrix is to select only those columns that match best with simulation (highest MAC value) thereby neglecting the redundant columns, see Fig. 13(a).

Fig. 13(b) shows the simulated FRF of the modal model, with three areas for dominant resonant peaks. The same areas are also marked in Fig. 13(a) by the white dashed lines. The strong correlation of the off-diagonal elements in I and III indicate local modes. The similarity of the modes in III becomes apparent from Fig. 14.

The high MAC values in the main diagonal in I and III indicate the high degree of similarity of measured and calculated mode shapes. For mode shape validation, MAC values above 0.8 are commonly considered to indicate good correlation [42]. The results summarised in Table 4 show MAC values above 0.8 and a frequency deviation of less than 14% for these modes. The outlier at 142.8 Hz represents a numerical mode, sensitive to the stiffness of the air bearings, which are modelled as linear bushings with stiffness values derived from nominal system pressure (see Eq. (5)). The sensitivity analysis shows that stiffness variations, i.e. from pressure fluctuations, can significantly shift the corresponding natural frequency.

The two modes in III show an increased frequency deviation despite high mode shape correlation. As mentioned in Section 3.4, these modes are very sensitive to the elasticity of the disc cover.

The modes in II have many cross-correlations, occasional MAC values slightly below 0.8 on the main diagonal and frequency deviations up to 20%. This behaviour is attributed to a high modal density combined with local modes dominated by movement of the discs. These localised modes are clearly resolved in the numerical simulations but cannot be fully captured by the 3D-SLDV measurements due to restricted access to vibration-relevant surfaces. As a result, experimentally measured responses in this frequency range are spatially similar, which leads to increased mode shape cross correlation and frequency deviation. Exactly the same effect can be obtained from the FE model when only sections corresponding to the measurement areas are considered in the MAC calculation, rather than the full mesh. In this case, the correlation matrix exhibits similar cross-correlations to the experimental results, indicating that the observed deviations primarily arise from measurement accessibility rather than modelling shortcomings. In addition, the sensitivity analysis shows that resonances in II

Table 4
Comparison between the simulated frequencies f_S and measured frequencies f_M with relative frequency error ϵ_f, MAC values, as well as damping parameters ζ_{FRF} identified by FRF adjustment.

Area	f_S (Hz)	f_M (Hz)	ϵ_f (%)	MAC (–)	ζ_{FRF} (%)
I	125.8	124.6	−0.95	0.91	2.0
	142.8	123.3	−13.66	0.92	1.2
II	255.6	280.9	9.90	0.90	4.0
	261.4	278.1	6.39	0.78	4.0
	274.7	252.8	−7.97	0.82	4.0
	290.0	233.6	−19.45	0.65	4.0
	303.3	301.1	−0.73	0.79	2.0
	310.1	273.7	−11.74	0.76	2.0
	325.7	298.6	−8.32	0.85	1.8
	332.1	272.6	−17.92	0.72	1.8
	332.6	357.6	7.52	0.70	1.8
III	1285.5	1119.4	−12.92	0.81	1.5
	1285.8	1129.9	−12.12	0.84	1.5

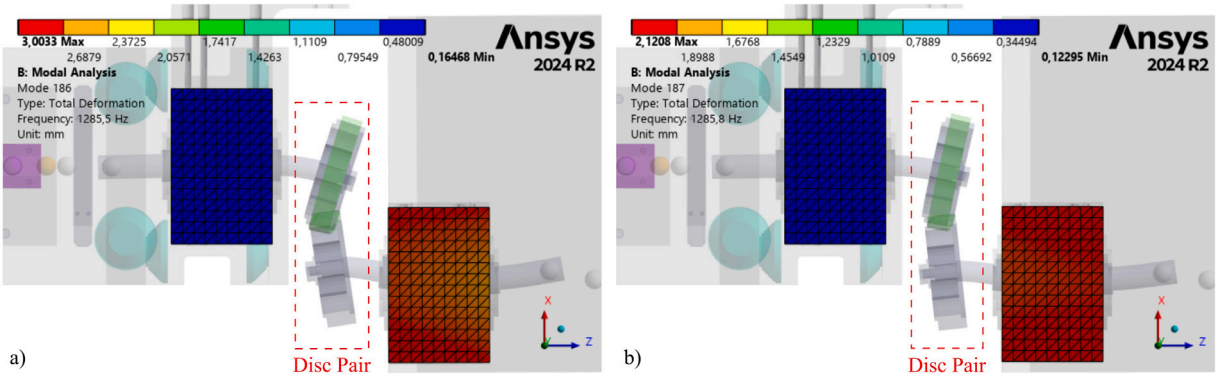

Fig. 14. Illustration of finite element modes (a) 1285.5 Hz (b) 1285.8 Hz. The surfaces which can be validated against the vibrometer measurement are shown in colour. The simulation reveals significant amplitudes on the discs that are not directly observable in the experimental setup. The deformations are not physically scaled.

are sensitive to air bearing stiffness and disc contact friction, such that small variations in operating conditions under operational excitation contribute to the observed frequency scatter (see Fig. 10(b) and Fig. 11(a) and (b)). Despite these effects, the dominant contact-relevant resonances in this frequency range are consistently identified in both simulation and measurement (see Fig. 12), which is the primary requirement for the present study.

The modal damping ratios ζ_{FRF} given in Table 4 result from manual FRF curve fitting, and they are in a plausible range of 1–4% for structural mechanical systems.

In order to illustrate the strong coupling of modes in III, the corresponding FE mode shapes (1285.5 Hz and 1285.8 Hz) are displayed in Fig. 14. The red and blue surfaces indicate the areas used for MAC calculation, as measurements on the discs are not possible. Only the simulation reveals significant amplitudes on structural components that are not directly observable in the experimental setup.

Using the updated FE model, it is furthermore possible to estimate the dynamic interaction forces in the contact. This knowledge is essential for the description of the tribological contact and the resulting effects. Since the dynamic contact force cannot be captured experimentally, the FE model renders substantially more insight into the understanding of the tribological effects than measurements of the time averaged preload force.

3.6. Limitations and scalability

The validated FE model is specific to the investigated twin-disc tribometer configuration and to the soft-nip calendering use case considered in this study. Accordingly, the absolute resonance frequencies and mode shapes identified here cannot be directly transferred to tribometers with substantially different geometries, boundary conditions or operating regimes.

However, the underlying workflow and modelling strategy are transferable. The sensitivity analysis distinguishes between system-level parameters that govern the structural dynamics of the test rig (e.g. air bearing stiffness) and specimen-specific parameters (e.g. disc cover stiffness), which affect primarily the contact-relevant modes in the high-frequency range. These parameter categories are expected to remain relevant for other twin-disc tribometer designs and related applications, such as wheel–rail or rolling–sliding contact studies, even though their quantitative influence will differ.

4. Conclusion and outlook

This study presents a workflow for dynamic modelling and experimental validation of tribological test rigs, demonstrated for a twin-disc tribometer. A comprehensive FE model is developed, incorporating detailed geometry, bolt pretension, nonlinear contact, nonlinear joints and rigid body components. The dynamic behaviour of the FE model is validated against modal parameters obtained from 3D-SLDV measurements, supported by an automated procedure for efficient comparison across several measurement configurations.

The comparison of simulated and experimentally identified modal parameters shows good agreement, and the validated model reproduces the frequency shifts observed for different disc covers. In addition to capturing the global dynamic behaviour, the model reveals critical structural components and parameter dependencies that are not accessible from measurements alone.

A key outcome is the identification of vibration modes with high modal contact forces that coincide with the frequency range in which

barring is observed experimentally. The sensitivity analysis shows that variations in disc cover stiffness, disc contact friction and air bearing stiffness directly influence these resonance frequencies, providing a mechanical explanation for the experimentally observed changes in chatter mark spacing across different covers. The model therefore provides a connection between machine dynamics and barring formation.

The present model does not account for thermally or velocity-dependent friction effects, which may become relevant under sustained sliding and frictional heating. Capturing such effects requires a transient contact formulation with evolving stick–slip conditions and temperature-dependent friction laws. The validated FE model developed in this work provides the structural-dynamic foundation for such extensions and will be coupled with a MBS model incorporating advanced contact models in future digital-twin developments.

The insights gained from this digital-twin approach will improve the interpretation of tribological test results and help integrate structural dynamics more effectively into tribometer design and optimisation.

CRediT authorship contribution statement

G. Brunbauer: Writing – original draft, Visualization, Validation, Software, Project administration, Methodology, Funding acquisition, Formal analysis, Data curation, Conceptualization. **M.J. Hochrainer:** Writing – review & editing, Supervision, Resources, Funding acquisition, Conceptualization. **S. Krenn:** Writing – review & editing, Project administration, Funding acquisition, Conceptualization. **A.M. Puhwein:** Writing – review & editing, Investigation, Data curation. **M.S. Bonney:** Writing – review & editing, Supervision. **S.J. Eder:** Writing – review & editing, Supervision, Funding acquisition. **P.A. Fotiu:** Writing – review & editing, Supervision, Conceptualization.

Declaration of Generative AI and AI-assisted technologies in the writing process

During the preparation of this work the author used ChatGPT/AI and DeepL/Translator in order to summarise literature and translate paragraphs written in German into scientific English. After using these tools, the authors reviewed and edited the content as needed and take full responsibility for the content of the published article.

Declaration of competing interest

The authors declare that they have no known competing financial interests or personal relationships that could have appeared to influence the work reported in this paper.

Acknowledgements

The presented results were realised as part of the COMET Centre InTribology (FFG no. 906860), a project of the “Excellence Centre for Tribology” (AC2T research GmbH). InTribology is funded within the COMET – Competence Centres for Excellent Technologies Programme by the federal ministries BMIMI and BMWET as well as the federal states of Niederösterreich and Vorarlberg based on financial support from the project partners involved. COMET is managed by The Austrian Research Promotion Agency (FFG). The authors acknowledge the “Gesellschaft für Forschungsförderung Niederosterreich m.b.H.” through its FTI PhD Funding Programme (FTI23-D-028) for the financial support. We acknowledge B. Nebel for the development of the SSI-based OMA algorithm, which was used for measurement identification. Open access funding was provided by TU Wien.

Data availability

Data will be made available on request.

References

[1] Holmberg K, Erdemir A. Influence of tribology on global energy consumption, costs and emissions. Friction 2017;5(3):263–84. http://dx.doi.org/10.1007/s40544-017-0183-5, Publisher: Tsinghua University Press.

[2] Ngo A, Handschuh M. An experimental investigation on the effect operating procedure has on tribometer measurements. In: IDETC-CIE2024. 2024 international power transmission and gearing conference (PTG), vol. 10, 2024, p. 123. http://dx.doi.org/10.1115/DETC2024-143520, V010T10A014.

[3] Ramalho A, Vilhena L. Experimental approach in tribology: Effects of test equipment dynamic response on the reliability and reproducibility of the results. Wear 2025;571:205770. http://dx.doi.org/10.1016/j.wear.2025.205770.

[4] Prost J, Boidi G, Lebersorger T, Varga M, Vorlaufer G. Comprehensive review of tribometer dynamics-Cycle-based data analysis and visualization. Friction 2022;10(5):772–86. http://dx.doi.org/10.1007/s40544-021-0534-0.

[5] Li S, Kolivand A, Shi Z, Anisetti A. On the tribo-dynamics of lubricated point contacts: modeling and experiment. Nonlinear Dynam 2023;111(11):10011–23. http://dx.doi.org/10.1007/s11071-023-08390-1.

[6] Li Z, Wang X, Zhang Q, Guan Z, Mo J, Ouyang H. Model reduction for friction-induced vibration of multi-degree-of-freedom systems and experimental validation. Int J Mech Sci 2018;145:106–19. http://dx.doi.org/10.1016/j.ijmecsci.2018.06.039.

[7] Hu Y, Wang W, Watson M, Six K, Al-Maliki H, Meierhofer A, Lewis R. Wear of driving versus driven discs in a twin disc rolling-sliding test. Wear 2023;512–513:204528. http://dx.doi.org/10.1016/j.wear.2022.204528.

[8] Zhou Y, Peng J, Wang W, Jin X, Zhu M. Slippage effect on rolling contact wear and damage behavior of pearlitic steels. Wear 2016;362–363:78–86. http://dx.doi.org/10.1016/j.wear.2016.05.001.

[9] Nunhez RDS, Gay Neto A. Numerical investigation for creep curve evaluation on a twin-disc test scenario using finite elements. J Braz Soc Mech Sci Eng 2021;43(7):339. http://dx.doi.org/10.1007/s40430-021-03042-0.

[10] Meneghetti G, Terrin A, Giacometti S. A twin disc test rig for contact fatigue characterization of gear materials. Procedia Struct Integr 2016;2:3185–93. http://dx.doi.org/10.1016/j.prostr.2016.06.397.

[11] Matkovič S, Pogačnik A, Kalin M. Wear-coefficient analyses for polymer-gear life-time predictions: A critical appraisal of methodologies. Wear 2021;480–481:203944. http://dx.doi.org/10.1016/j.wear.2021.203944.

[12] Wiendl S. Modellierung von schwingungsphänomenen in papierkalandern (Ph.D. thesis), Darmstadt: Technische Universität Darmstadt; 2011, URL: http://tuprints.ulb.tu-darmstadt.de/2833/.

[13] Puhwein AM, Jakab B, Haslehner C, Florian W, Thalhammer V, Hochrainer MJ, Vorlaufer G, Varga M. Investigation of the dynamic influences of a two-disc tribometer on wear via high-end cameras and vibrometers. In: Baqersad J, Di Maio D, Rohe D, editors. Computer vision & laser vibrometry. vol. 6, Cham: Springer Nature Switzerland; 2025, p. 69–83. http://dx.doi.org/10.1007/978-3-031-68192-9_8, URL: https://link.springer.com/10.1007/978-3-031-68192-9_8, Series Title: Conference Proceedings of the Society for Experimental Mechanics Series.

[14] Peesapati SK, Prost J, Vorlaufer G, Varga M, Gachot C. Chatter detection and identification based on mode decompositions. Adv Eng Mater 2025;2500382. http://dx.doi.org/10.1002/adem.202500382.

[15] Weekes B, Ewins D. Effective use of scanning laser doppler vibrometers for modal testing. In: Allemang R, editor. Topics in modal analysis II. vol. 8, Cham: Springer International Publishing; 2014, p. 43–58. http://dx.doi.org/10.1007/978-3-319-04774-4_5, URL: https://link.springer.com/10.1007/978-3-319-04774-4_5, Series Title: Conference Proceedings of the Society for Experimental Mechanics Series.

[16] Yan S, Li B, Li F, Li B. Finite element model updating of liquid rocket engine nozzle based on modal test results obtained from 3-D SLDV technique. Aerosp Sci Technol 2017;69:412–8. http://dx.doi.org/10.1016/j.ast.2017.07.002, URL: https://linkinghub.elsevier.com/retrieve/pii/S1270963816304850.

[17] Rohe DP. Using high-resolution measurements to update finite element substructure models. In: Di Maio D, editor. Rotating machinery, vibro-acoustics & laser vibrometry. vol. 7, Cham: Springer International Publishing; 2019, p. 137–48. http://dx.doi.org/10.1007/978-3-319-74693-7_13, URL: http://link.springer.com/10.1007/978-3-319-74693-7_13, Series Title: Conference Proceedings of the Society for Experimental Mechanics Series.

[18] Alarcón DJ, Sampathkumar KR, Paeschke K, Mallareddy TT, Angermann S, Frahm A, Rüther-Kindel W, Blaschke P. Modal model validation using 3D SLDV, geometry scanning and FEM of a multi-purpose drone propeller blade. In: Di Maio D, Castellini P, editors. Rotating machinery, hybrid test methods, vibro-acoustics & laser vibrometry. vol. 8, Cham: Springer International Publishing; 2017, p. 13–22. http://dx.doi.org/10.1007/978-3-319-54648-3_2, URL: http://link.springer.com/10.1007/978-3-319-54648-3_2, Series Title: Conference Proceedings of the Society for Experimental Mechanics Series.

[19] Puhwein AM, Biederbeck A, Jakab B, Varga M. Experimental modal analysis of a twin-disc tribometer usinga 3D-scanning laser Doppler vibrometer. In: Computer vision & laser vibrometry. vol. 6, Orlando, Florida: River Publishers; 2025, p. 103–10. http://dx.doi.org/10.13052/97887-438-0151-1_12, URL: https://www.riverpublishers.com/research_article_details.php?book_id=1466&cid=12.

[20] Ruggiero A, Sicilia A. Implementation of a finite element deformation model within an elasto-hydrodynamic lubrication numerical solver for a ball in socket tribopair. Front Mech Eng 2022;8:909156. http://dx.doi.org/10.3389/fmech.2022.909156.

[21] Waddad Y, Magnier V, Dufrénoy P, De Saxcé G. Multiscale thermomechanical modeling of frictional contact problems considering wear – Application to a pin-on-disc system. Wear 2019;426–427:1399–409. http://dx.doi.org/10.1016/j.wear.2018.12.063.

[22] Mehrabi R, Salimi M, Ziaei-Rad S. Finite element analysis on chattering in cold rolling and comparison with experimental results. J Manuf Sci Eng 2015;137(6):061013. http://dx.doi.org/10.1115/1.4030379.

[23] Ansys, Inc, GmbH D. ANSYS optiSLang. 2024, URL: https://www.ansys.com/products/connect/ansys-optislang.

[24] Polytec GmbH. PSV Software. 2025, URL: https://www.polytec.com/int/vibrometry/products/software/psv-software.

[25] The MathWorks, Inc. MATLAB. 2024, URL: https://de.mathworks.com/products/matlab.html.

[26] Brincker R, Ventura CE. Introduction to operational modal analysis. 1st ed.. Wiley; 2015, http://dx.doi.org/10.1002/9781118535141, URL: https://onlinelibrary.wiley.com/doi/book/10.1002/9781118535141.

[27] VDI - Verein Deutscher Ingenieure, VDE - Verband der Elektrotechnik Elektronik Informationstechnik. Entwicklung cyber-physischer mechatronischer Systeme (CPMS) / Development of mechatronic and cyber-physical systems. 2021, URL: https://www.vdi.de/richtlinien/programme-zu-vdi-richtlinien/vdi-2206, ICS: 03.100.40; 31.220.01; 39.020. Ersetzt VDI 2206:2004-06.

[28] Kerschen G, Worden K, Vakakis A, Golinval J-C. Nonlinear system identification in structural dynamics: Current status and future directions. Conference proceedings of the society for experimental mechanics series, 2007.

[29] Noël J, Kerschen G. Nonlinear system identification in structural dynamics: 10 more years of progress. Mech Syst Signal Process 2017;83:2–35. http://dx.doi.org/10.1016/j.ymssp.2016.07.020.

[30] Popov VL. Kontaktmechanik und reibung: Von der nanotribologie bis zur erdbebendynamik. Berlin, Heidelberg: Springer Berlin Heidelberg; 2015, http://dx.doi.org/10.1007/978-3-662-45975-1, URL: https://link.springer.com/10.1007/978-3-662-45975-1.

[31] Gebhardt C. Praxisbuch FEM mit ANSYS Workbench: Einführung in die lineare und nichtlineare mechanik. Hanser eLibrary, 3., aktualisierte Auflage. München: Hanser; 2018, http://dx.doi.org/10.3139/9783446457409.

[32] Delli Carri A, Weekes B, Di Maio D, Ewins D. Extending modal testing technology for model validation of engineering structures with sparse nonlinearities: A first case study. Mech Syst Signal Process 2017;84:97–115. http://dx.doi.org/10.1016/j.ymssp.2016.04.012, Publisher: Elsevier BV.

[33] Cooper SB, DiMaio D, Ewins DJ. Integration of system identification and finite element modelling of nonlinear vibrating structures. Mech Syst Signal Process 2018;102:401–30. http://dx.doi.org/10.1016/j.ymssp.2017.09.031, Publisher: Elsevier BV.

[34] VDI - Verein Deutscher Ingenieure. Systematische berechnung hochbeanspruchter schraubenverbindungen / systematic calculation of high duty bolted joints. 2015, URL: https://www.vdi.de/richtlinien/unsere-richtlinien-highlights/vdi-2230.

[35] Rust W. Nichtlineare finite-elemente-berechnungen mit ANSYS workbench: Strukturmechanik: Kontakt, material, Große verformungen. Wiesbaden: Springer Fachmedien Wiesbaden GmbH; 2020.

[36] Wriggers P. Computational contact mechanics. 2nd ed.. Berlin ; New York: Springer; 2006.

[37] SKF Group. SimPro Quick. 2017, URL: https://www.skf.com/group/digital-tools/select-and-evaluate/simpro-quick.

[38] SKF Group. SKF bearing app für ANSYS mechanical. 2023, URL: https://catalog.ansys.com/product/63497ec83c6398b6fea1184a/skf-bearing.

[39] Koblar D, Boltežar M. Evaluation of the frequency-dependent Young's modulus and damping factor of rubber from experiment and their implementation in a finite-element analysis. Exp Tech 2016;40(1):235–44. http://dx.doi.org/10.1007/s40799-016-0027-7.

[40] Eldred MS, Venkayya VB, Anderson WJ. Mode tracking issues in structural optimization. AIAA J 1995;33(10):1926–33. http://dx.doi.org/10.2514/3.12747.

[41] Ansys, Inc. ANSYS Workbench. 2024, URL: https://www.ansys.com/.

[42] Ewins DJ. Modal testing: theory, practice and application. Mechanical engineering research studies engineering dynamics series, 2nd ed.. Baldock: Research Studies Press; 2000, Number 10.

[43] Zhang E, Pintelon R, Guillaume P. Modal identification using OMA techniques: Nonlinearity effect. Shock Vib 2015;2015:1–12. http://dx.doi.org/10.1155/2015/178696.

[44] Möser M. Modalanalyse. Fachwissen technische akustik, Berlin, Heidelberg: Springer Berlin / Heidelberg; 2020.